An improved stall prediction model for axial compressor stage based on diffuser analogy

An improved stall prediction model for axial compressor stage based on diffuser analogy

Jian Li[a], Jinfang Teng[a,*],Michele Ferlauto[b], Mingmin Zhu[a], Xiaoqing Qiang[a]

[a]*School of Aeronautics and Astronautics, Shanghai Jiao Tong University, China*

[b]*Department of Mechanical and Aerospace Engineering, Politecnico di Torino, Italy*

**Corresponding author email: tjf@sjtu.edu.cn*

Abstract:

Stall represents a limit to the useful operation of the axial compressor. Despite its difficulty, a rational and effective stall prediction model is an urgent requirement for compressor designers. In this paper, a stall prediction model for determining the maximum static pressure rise capability of axial flow compressor stage is presented based on Koch's two dimensional diffuser analogy concept. Compared with the original Koch's model, where the flow angles are only used to consider the increase of inlet dynamic pressure factor caused by high stagger angle, this paper takes into account the effect of flow angles on the diffusion length, and derives the mathematical expression of the modified non-dimensional diffusion length. A semi-empirical correlation is presented to account for the effect of camber angle on the stalling static-pressure-rise coefficient of axial compressor stages. By re-evaluating the Reynolds number effect, a blockage indicator is proposed to determine the effect of boundary layer blockage on stalling capability. Good agreement is demonstrated between the predicted and test stalling pressure rise data for a wide range of axial compressor stages and a 4-stage low speed research compressor. Compared with the original Koch's model, the relative error of the modified model in predicting the stall margin is reduced from 22% to 5%. This model has a guiding significance for the selection of initial design variables in the axial compressor design process.

Keywords: Axial compressor; Stall prediction; Empirical model; Static pressure rise

1. Introduction

Stall and surge are described as the most serious problems in axial flow compressors. The occurrence of stall or surge in an engine-type compressor will lead to a large drop in performance, and even structural damage[1]. It was found by Day[2] that stall not only precedes surge, but also causes surge, therefore, the stall is the actual one that constrains the operating range of the axial compressors. Over the past 80 years, much effort has been devoted to understand and avoid these unstable phenomena in axial compressors. We have discovered two types of stall inception: modes[3] and spikes[4], and various stalling mechanisms, such as the tip clearance flow, the radial vortices and the leading edge shed vortex. However, as the stall is such a difficult problem, the axial compressors may differ from one another in stall inception features[5-9], which makes the stall warning for a new compressor seem unlikely. Despite the difficulties, a rational stall prediction method has been the goal pursued tirelessly by the compressor designers considering the urgent requirements and high rewards.

Many models for predicting the onset of axial compressor stall have been put forward in the literatures. In principle, these stall prediction models can be summed up as coming under three

categories: small perturbation theory, nonlinear finite disturbance theory and the empirical correlations. The small perturbation theory was first given by Emmons[10], in which a small amplitude perturbation is superimposed on the given steady operation conditions of a compressor to predict the rotating stall. Although the small perturbation theory has achieved some success in predicting the propagation speed of the rotating stall, it has become clear that in the fully developed rotating stall regime, the stall cells are definitely not small disturbances and the small perturbation theory is inapplicable. In other words, the small perturbation theory can show whether a compressor is stable, but not how stable. To follow the subsequent development of the small perturbations to fully developed stall cells, Takata and Nagano[11], Stenning[12], and Fabri[13] all proposed their nonlinear models based on the nonlinear finite disturbance theory. The nonlinear models are capable of predicting the post-stall transients by using time matching techniques, however, this also makes the nonlinear models very complex and some important fully stalled features are still not modeled well. Although the small perturbation theory and nonlinear finite disturbance theory have played an important role in the understanding of the physical mechanisms of rotating stall, they are rarely used as stall prediction tools by compressors designers. Because before the linear or nonlinear calculations are possible, one must be able to predict the detailed compressor performance characteristics, and at present this cannot be done with sufficient accuracy. A comment on the above two methods was given by Zika[14], who stated that "the linear and nonlinear methods are actually test analyzers rather than predictors for stall inception". Thus, in current axial compressors design practice, the widely used stall prediction models are the empirical correlations.

The basic concept of empirical correlations is to give a parameter that correlates the onset of stall with different compressors geometric and aerodynamic variables. Then the parameter could be applied at different spanwise locations or meanline to limit the maximum loading of compressor blade row or stage. Several attempts have been made to find the stall indicators: the diffusion factor D proposed by Lieblein[15] is one of the well-known stall indicators. In the context of low speed two-dimensional (2D) cascade experimental results, Lieblein found the profile loss correlated quite well with the diffusion factor, and there was a sharp increase in profile loss when the diffusion factor was greater than 0.6. Thus $D \succ 0.6$ could be taken as the stall criterion for compressor cascades. Although the D-factor is still much in use[16-19], it is quite common to observe values of D-factor well in excess of 0.6 at operating points away from the surge line, or for the compressors with a large aspect ratio, stall often occurs at the blade tip without being affected much by D-factor. Another common stall criterion was proposed by de Haller[20] that $W_2/W_1 \prec 0.72$. It is now generally accepted that this criterion is a stall indicator related to the boundary layer separation at the endwall of the blades, and there is considerable experimental evidence that de Haller number is more effective than D-factor. But, again, a large number of exceptions are encountered where de Haller numbers are well below 0.72 at operating points that are quite far from the surge line.

The most comprehensive empirical correlation for predicting stall is the two-dimensional diffuser analogy method proposed by Koch[21]. It is well known that the maximum static pressure rise coefficient of a two-dimensional diffuser could be correlated with its length-to-width ratio, and since both the diffuser and compressor work by diffusing the fluid, the stalling static pressure rise coefficient of the compressor could also be modeled by parameters similar to those used for the diffuser. The diffuser analogy method has been proven to be very effective for stall prediction of a large number axial compressor by Koch and Schweitzer[22], the latter of whom calculated the stall margin of static pressure rise coefficient from peak efficiency by a conical diffuser analogy. The

stall prediction correlations based on diffuser analogy have been intensively studied by aero-engine companies such as General Electric[23] and Pratt & Whitney, and are still in use today[14]. However, they are regarded as the core technology and trade secret, and there is little information in the open literatures.

This paper is an attempt to improve the applicability of Koch's stalling static pressure rise model to axial compressor stages. It will be shown that how the flow angles affect the compressors diffusion length, and a detailed mathematical derivation of the non-dimensional diffusion length will be given. A blockage indicator is proposed to re-evaluate the correction of Reynolds number for the stalling static pressure rise coefficient.

2. Diffuser analogy

The performance for two-dimensional diffuser is often presented as shown in Fig.1[24], in which the contour plots of static-pressure-rise coefficient as a function of area ratio and length-to-width ratio are made for a given inlet boundary layer thickness. In a prescribed non-dimensional diffuser length, there is an area ratio producing maximum static-pressure-rise, further increase in the area ratio will reduce the pressure rise by resulting in more separated flow.

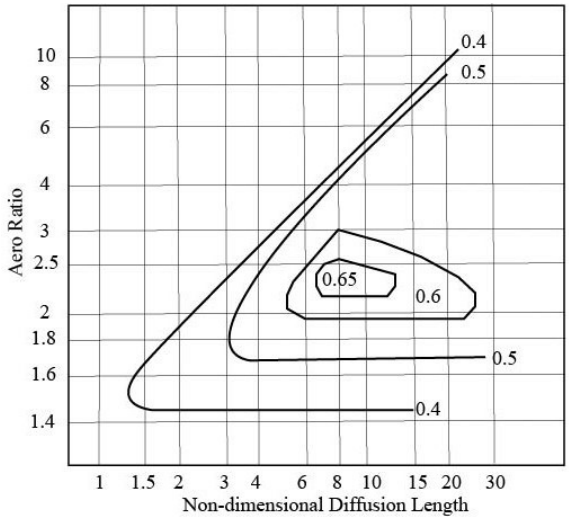

Figure 1. Performance chart for two-dimensional diffusers[24]

Koch reasoned since the compressor cascade functions by diffusing the fluid, it is in essence a diffuser and therefore the maximum static-pressure-rise coefficient of a compressor cascade could also be correlated with parameters analogous for the two-dimensional diffuser as shown in Fig.2.

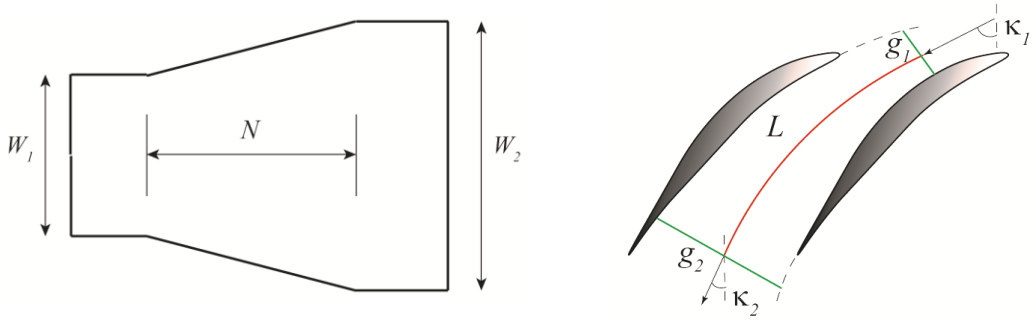

(a) Two-dimensional diffuser (b) Compressor cascade

Figure 2. Analogy between compressor cascade and 2D diffuser

In the diffuser analogy concept, the cambered airfoil length of a compressor cascade is taken as the diffusing length:

$$L = \frac{C\dfrac{2\pi}{360}\dfrac{\phi}{2}}{\sin\dfrac{\phi}{2}} \tag{1}$$

Where, C is the midspan chord length, ϕ is the midspan camber angle in deg. The width used for a compressor cascade is the exit flow area, as it remains approximately constant over the entire operating range and is approximately equal to the exit staggered spacing between adjacent blades:

$$g_2 = S\cos\kappa_2 \tag{2}$$

Where S is the tangential spacing between adjacent blades, κ_2 is the exit blade angle. Thus the equivalent length-to-width ratio for a compressor cascade could be expressed as:

$$\frac{L}{g_2} = \frac{C\dfrac{2\pi}{360}\dfrac{\phi}{2}}{S\sin\dfrac{\phi}{2}\cos\kappa_2} \tag{3}$$

Then the equivalent length-to-width values of the rotor and stator are combined into a weighted average stage value with the blade row inlet dynamic head as a weighting factor:

$$\left(\frac{L}{g_2}\right)_{stage} = \frac{\left(\dfrac{L}{g_2}V_1'^2\right)_{rotor} + \left(\dfrac{L}{g_2}V_1^2\right)_{stator}}{\left(V_1'^2\right)_{rotor} + \left(V_1^2\right)_{stator}} \tag{4}$$

The stalling static-pressure-rise coefficient for the baseline configurations could be given by the two-dimensional diffuser correlation of Sovran and Klomp[25] at 9% inlet boundary layer blockage, in which the baseline configurations are the axial compressor stages with Re=130000, 5.5% ε/g and 0.38 $\Delta z/s$. The effects of Reynolds number, blade tip clearance and blade row axial spacing on the stalling static-pressure-rise coefficient are accounted for through the other three correlations in Fig. 3.

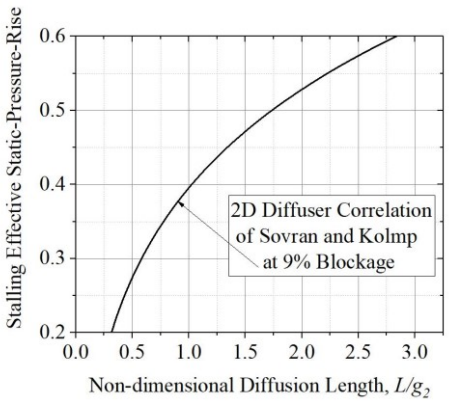

(a) Correlation for baseline

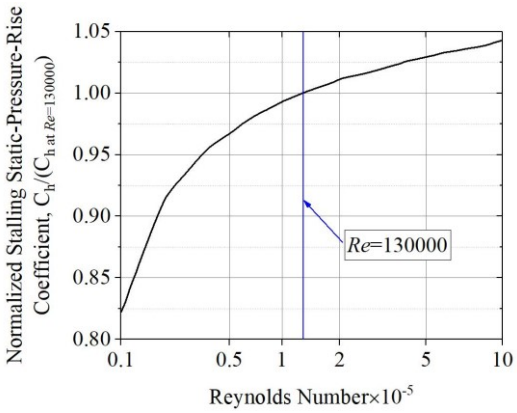

(b) Effect of Reynolds number

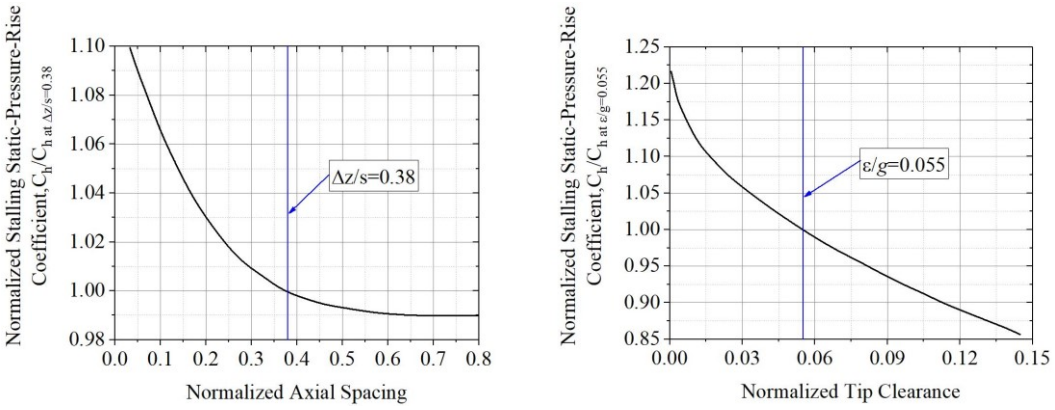

(c) Effect of axial spacing (d) Effect of tip clearance

Figure 3. Correlation of stalling static-pressure-rise coefficient, adapted from Koch[21]

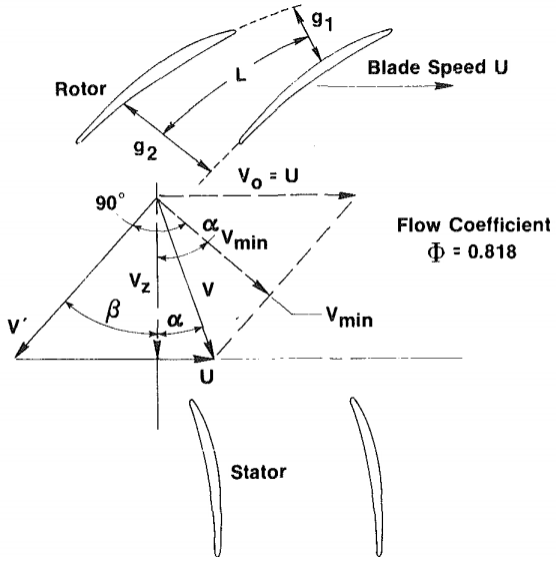

Figure 4. Definition of dynamic pressure factor[21]

The final adjustment to the stalling static-pressure-rise coefficient described by Koch is to account for the effect of blade stagger on the compressor performance. It was found by Koch that the axial compressor stages with high stagger angles experience an increase in relative velocity into the downstream row due to the change in frame of reference, as shown in Fig.4, and this gives rise to stalling static-pressure-rise coefficient.

Thus the effect of blade stagger on the stalling pressure rise coefficient is implicitly accounted for through the effective dynamic head:

$$F_{ef} = \frac{V^2 + 2.5V_{\min}{}^2 + 0.5U^2}{4V^2} \tag{5}$$

Where V is the stator inlet absolute velocity, U is the blade speed, V_{min} is the minimum possible blade row inlet velocity in the presence of upstream wakes:

$$V_{\min} = \begin{cases} V\sin(\alpha+\beta) & \text{if } (\alpha+\beta) \le 90^\circ \text{ and } \beta \ge 0^\circ \\ V & \text{if } (\alpha+\beta) > 90^\circ \\ U & \text{if } \beta \le 0^\circ \end{cases} \tag{6}$$

At this point, the maximum pressure rise potential of an axial compressor stage could be calculated from the maximum static-pressure-rise of baseline compressor $C_{h,adj}$, which can be read from Fig.3(a), Reynolds number correction factor F_{Re}, rotor tip clearance correction factor $F_{\varepsilon/g}$,

blade row axial gap correction factor $F_{\Delta z/s}$ and the effective dynamic head:

$$C_{h,\max} = C_{h,adj} F_{\mathrm{Re}} F_{\varepsilon/g} F_{\Delta z/s} F_{ef} \tag{7}$$

The actual static-pressure-rise coefficient $C_{h,act}$ at the design speed for a compressor stage could be calculated by Equation (8). When $C_{h,\,act} \geq C_{h,max}$, the compressor stage is considered to have stalled and reached its limiting loading.

$$C_{h,act} = \frac{C_p T_1 \left[\left(p_2 / p_1 \right)^{(k-1)/k} - 1 \right]_{stage} - 0.5\left(U_2^2 - U_1^2 \right)}{0.5\left(V_{1\,rotor}^{'2} + V_{1stator}^2 \right)} \tag{8}$$

Where C_p is the specific heat at constant pressure, T_1 is the inlet static temperature, p is the static pressure, and k is the ratio of specific heats. In order to represent the static pressure rise coefficient of the compressor stages on the performance map of the two-dimensional diffuser, the actual static pressure rise coefficient $C_{h,act}$ is adjusted to the effective static pressure rise coefficient C_h according to Equation (7):

$$C_h = \frac{C_{h,act}}{F_{\mathrm{Re}} F_{\varepsilon/g} F_{\Delta z/s} F_{ef}} \tag{9}$$

Koch derived the stall prediction model from the test results of a large number of low speed compressor stages, thus its applicability is questionable, and indeed many experimental data have shown that Koch's model is somewhat unreliable as a quantitative design tool.

3. Effect of flow angles

In Koch's stall prediction model, the camberline (approximated by the meanline length of circular-arc airfoil) was taken as the diffusing length for compressor cascade, as shown is Fig. 2(b). However, as shown in Fig. 5, the diffusion length of the fluid through a blade passage will be affected by the inlet and outlet flow angles. As the inlet and outlet angles increase, the diffusion length will decrease resulting a smaller static-pressure-rise coefficient. And this explains why, in Koch's experience, the stalling static-pressure-rise coefficients of most axial compressor stages are below the values predicted by the diffuser correlation.

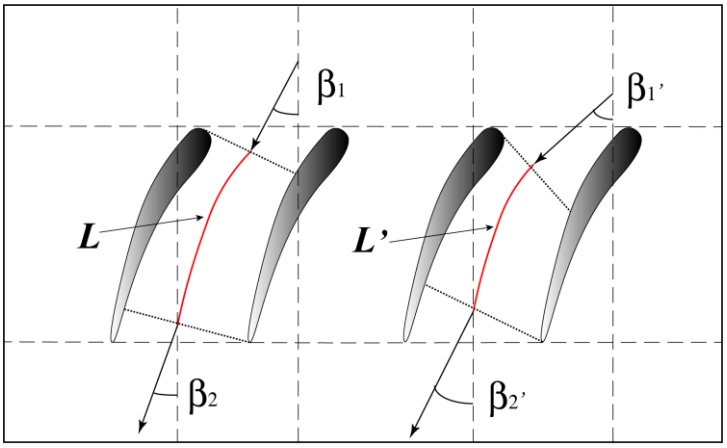

Figure 5. Effect of flow angle on diffusion length

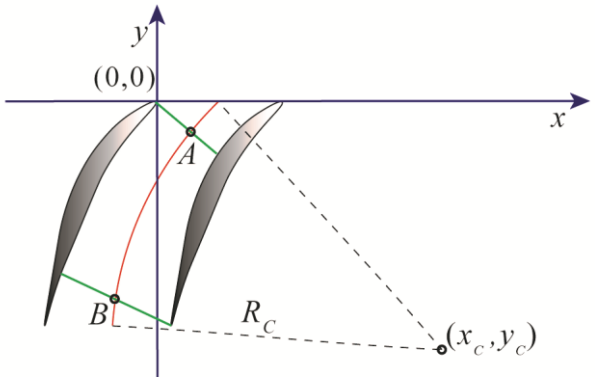

Figure 6. Schematic diagram giving definition of the modified diffusion length

Fig. 6 gives a description of the compressor cascade in Cartesian coordinate. It is clear that the actual diffusion length should be equal to *AB*, which depends on the camber angles at point A and B:

$$L = \frac{C\dfrac{2\pi}{360}\dfrac{\kappa_A - \kappa_B}{2}}{\sin\dfrac{\phi}{2}} \tag{10}$$

The camber angles κ_A and κ_B could be derived as follows:

First, the blade camberline is approximated as a circular-arc, and the blade passage centerline could be expressed as a part of the following circle:

$$\begin{cases} R_c = C/2/\sin(\phi/2) \\ x_c = R_c\cos\kappa_1 + S/2 \\ y_c = R_c\sin\kappa_1 \end{cases} \tag{11}$$

Where R_c is the radius of the circle, (x_c,y_c) is the coordinate of the circle center.

Expressing the inlet and outlet flow angles in terms of slope:

$$\begin{cases} k_1 = -\tan\beta_1 \\ k_2 = -\tan\beta_2 \end{cases} \tag{12}$$

Then, the coordinates of point A and B can be calculated:

$$\begin{cases} x_A = \dfrac{x_c + k_1 y_c - \sqrt{R_c^{\,2}\left(k_1^{\,2}+1\right) - \left(k_1 x_c - y_c\right)^2}}{k_1^{\,2}+1} \\ x_B = x_c - \dfrac{k_2 f(\beta_2) + \sqrt{R_c^{\,2}\left(k_2^{\,2}+1\right) - f^2(\beta_2)}}{k_2^{\,2}+1} \end{cases} \tag{13}$$

$$\begin{cases} y_A = k_1 x_A \\ y_B = k_2\left(x_B - x_c + S/2 - R_c\cos\beta_2\right) + y_c + R_c\sin\beta_2 \end{cases} \tag{14}$$

Where $f(\beta_2)$ is:

$$f(\beta_2) = k_2\left(R_c\cos\beta_2 - S/2\right) + R_c\sin\beta_2 \tag{15}$$

The camber angles κ_A and κ_B are:

$$\begin{cases} \kappa_A = a\tan\dfrac{y_A - y_c}{x_c - x_A} \\ \kappa_B = a\tan\dfrac{y_B - y_c}{x_c - x_B} \end{cases} \tag{16}$$

Finally, the modified non-dimensional diffusion length of a compressor cascade can be written as:

$$\left(\frac{L}{g_2}\right)_{\text{mod}} = \frac{\sigma\dfrac{2\pi}{360}\dfrac{\kappa_A - \kappa_B}{2}}{\sin\dfrac{\phi}{2}\cos\kappa_2} \tag{17}$$

Where σ is the solidity of compressor cascade.

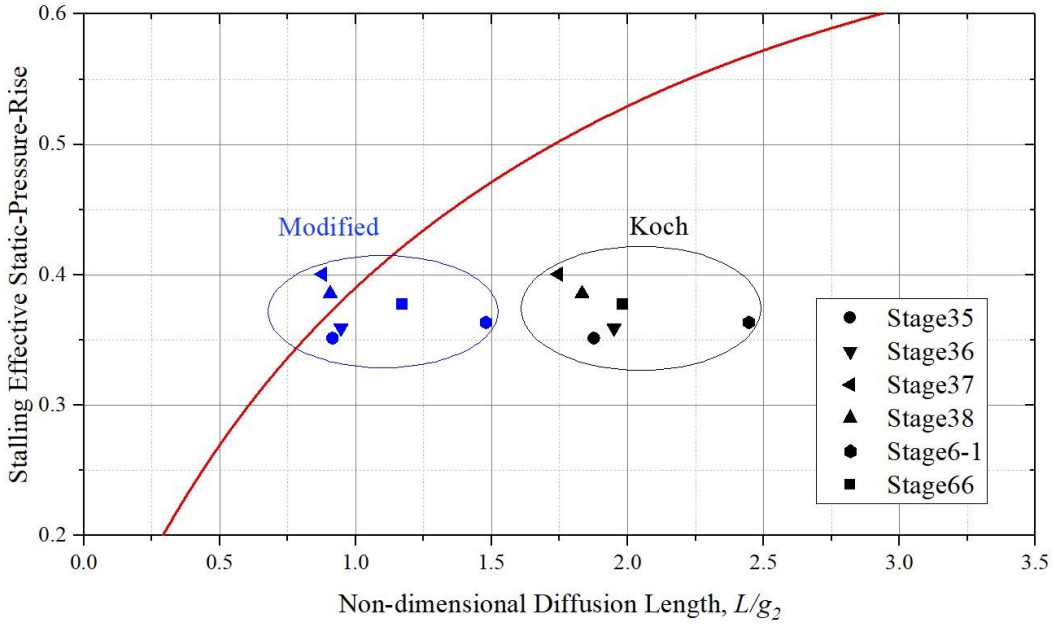

Figure 7. Correlation of static-pressure-rise coefficient considering flow angles effect

The stalling static-pressure-rise coefficients versus L/g_2 and $(L/g_2)_{mod}$ for 4 highly loaded axial compressor stages are shown in Fig. 7. It is seen that the modified non-dimensional diffusion length follows rather closely the trend of the 2D diffuser correlation at 9% inlet blockage. Although the prediction accuracy of the stall prediction model for the four high speed compressors is greatly improved by including the effect of flow angles on the diffusion length, this does not seem to be the case for the other compressors. Thus, some stall-related parameters should be re-evaluated to further improve the model. In addition, it is apparent from these data that the effect of airfoil camber on the static-pressure-rise coefficient is not the same as Koch's conclusion, where the camber angle has little effect on stalling static-pressure-rise at a fixed stagger angle. These will be investigated in detail in the next section.

4. Blockage indicator

In the development of stall prediction model, Koch used several low-speed compressor stages to evaluate the effect of Reynolds number on the stalling static-pressure-rise coefficient, and determined that the correlation of 2D diffuser with 9% inlet boundary layer blockage could be the stall limits for compressor stages working at Re=130000. Then the other compressors are adjusted

by the factor F_{Re} read from the curve in Fig. 3b. While the trend of the curve in Fig. 3b is theoretically reasonable, the effect of Reynolds number on the stall static-pressure-rise coefficient is oversimplified. And there seems to be a coincidence in using the correlation of two-dimensional diffuser with 9% blockage as a stall limit for compressor stages.

For the 2D diffuser, a large reduction in pressure-recovery will occur with increased thickness of turbulent inlet boundary layer. According to the turbulent boundary layer theory[26], the following relationship exists between the boundary layer thickness and Reynolds number:

$$\delta \propto \frac{1}{\mathrm{Re}^{1/6}} \tag{18}$$

It can be seen that as the Reynolds number decrease, so does the 2D diffuser pressure-recovery. A similar conclusion could also be found in compressors, where the stall performance becomes progressively independent of Re as the Re increases. Therefore, it is reasonable to take the correlations of 2D diffuser with variable blockage as the stall limits for axial compressor stages in different Reynolds number range. Inspired by this assumption, this paper proposes an effective blockage indicator for axial compressors to account for the effect of Reynolds number on stalling static-pressure-rise coefficient:

$$BL = \frac{\mathrm{Re}^{1/6}}{\sigma} \tag{19}$$

The blockage indicator is a parameter that indicates the blockage inside the compressor cascade, where Re reflects the thickness of the aerodynamic boundary layer and the solidity σ reflects the geometrical flow area of the compressor cascade. The thickness of the aerodynamic boundary layer increases as Re decreases, and the geometrical flow area of the compressor cascade decreases as the solidity σ increases. Therefore, it can be seen that the effective flow area in the compressor cascade passage will decreases with the decrease of *BL*, in other words, the smaller *BL* is, the larger the blockage in the compressor will be.

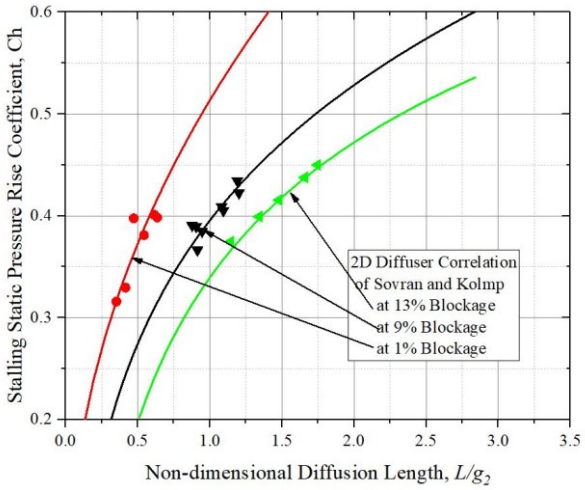

Figure 8. Correlations of static-pressure-rise coefficient at different blockage

Data from about 20 high speed axial compressor stages[27-41] at design speed were used to determine the effect of blockage indicator upon stall static-pressure-rise coefficient. The stalling pressure rise coefficients of these compressor stages are shown in Fig. 8, as well as the correlations of Sovran and Klomp for assumed inlet boundary layer thickness of 1 percent, 9 percent and 13 percent.

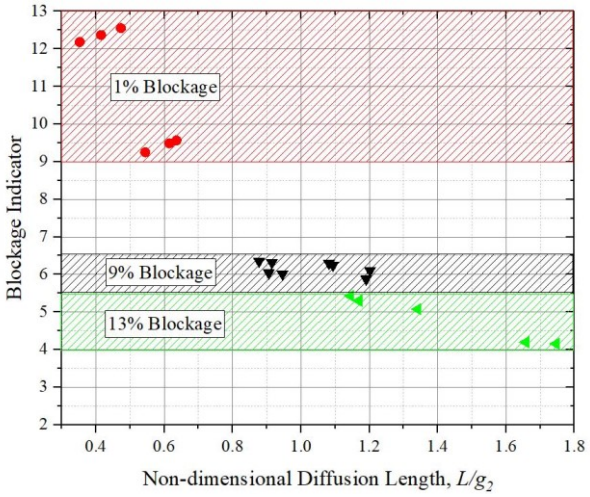

Figure 9. Effects of blockage indicator on static-pressure-rise coefficient

And Fig. 9 shows the results for blockage indicator *BL* versus non-dimensional diffusion length. It can be clearly seen that for compressors using the same inlet boundary layer thickness correlation as the stall limit, their blockage indicators are also within the same range. It's not surprising that the blockage indicator range for 1% blockage is much wider than for 9% and 13%, the point here is that as Reynolds number increases, the influence of Reynolds number on compressor performance gradually decreases.

The results in Fig. 8 have taken into account the effect of the camber angle on the stall static pressure rise coefficient. Since the camber angle mainly affects the geometry of the blade passage, the correlation of the camber effect in this paper is based on the ratio of the non-dimensional diffusion length under the actual camber angle to the reference angle:

$$F_{cam} = \left[\frac{L / g_2}{(L / g_2)_{ref}} \right]^2 \tag{20}$$

Where $(L/g_2)_{ref}$ is the non-dimensional diffusion length of the rotor with a reference camber angle, which is a function of stagger angle as shown in Fig. 10. By trial and error, a good data fitting in this paper was found to occur when the exponent on the right hand of equation (20) was 2.

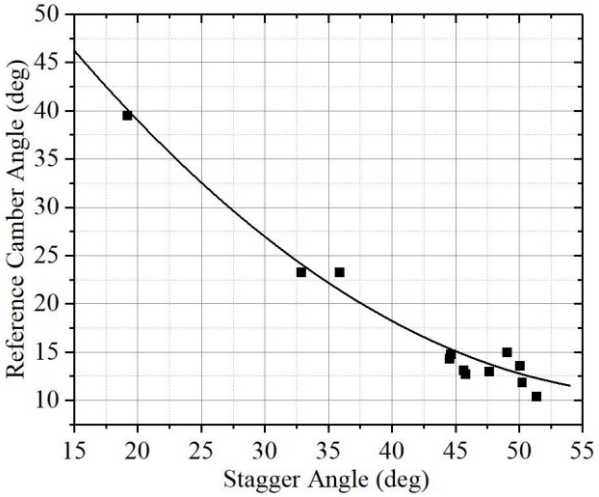

Figure 10. Correlation of reference camber angle

The formula for calculating the reference camber angle is as follows:

$$\phi_{ref} = 0.0165\zeta^2 - 2.029\zeta + 72.97 \tag{21}$$

Where ζ is stagger angle.

By combining equation (3) and equation (20), the adjustment factor F_{cam} can be expressed as follows:

$$F_{cam} = \left[\frac{\phi \sin\left(\phi_{ref}/2\right)\cos\left(\kappa_2 - 0.5\phi_{ref} + 0.5\phi\right)}{\phi_{ref}\sin\left(\phi/2\right)\cos\kappa_2} \right]^2 \tag{22}$$

5. Final correlation

The final form of the correlation for stalling static-pressure-rise coefficient is as follows:

$$C_{h,\max} = C_{h,\mathrm{mod}} F_{cam} F_{\varepsilon/g} F_{\Delta z/s} F_{ef} \tag{23}$$

Where $C_{h,mod}$ is determined by the blockage indicator BL and the modified non-dimensional diffusion length $(L/g_2)_{mod}$. When BL is obtained, the corresponding blockage interval can be found through Fig. 9 to determine which blockage curve in Fig.8 is suitable for the compressor stage. Then $C_{h,mod}$ can be read in Fig. 8 by $(L/g_2)_{mod}$. In order to demonstrate the proposed stall prediction model, the stalling static-pressure-rise coefficient correlations are compared to data from five high speed axial compressor stages[42-46], which are not included in the development of the stall prediction model. The comparisons of predicted and experimental static-pressure-rise coefficients are presented in Table 1, Fig.11 and Fig.12. The actual experimental static-pressure-rise coefficients are divided by the 4 correlation factors in Fig.11 and Fig.12, so they are different with the values in Table 1.

Table 1. Comparison of predicted and experimental static-pressure-rise coefficients

Number	Compressor stages	BL	$C_{h,act}$	$(C_{h,max})_{Koch}$	$(C_{h,max})_{mod}$
1	Stage G	7.34	0.4299	0.5255	0.3932
2	Fan stage	5.70	0.4929	0.6590	0.5399
3	PW-3772	6.32	0.4926	0.6170	0.5344
4	Stage 52	6.40	0.3335	0.3832	0.3238
5	Stgae51A	14.02	0.2714	0.3843	0.3100

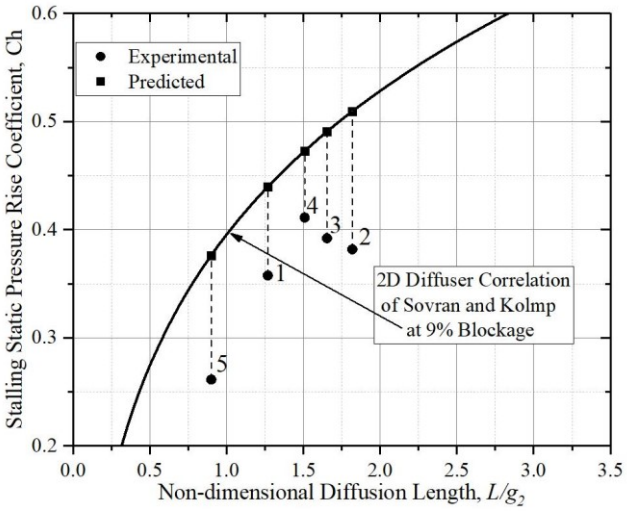

Figure 11. Predicted results of Koch's model

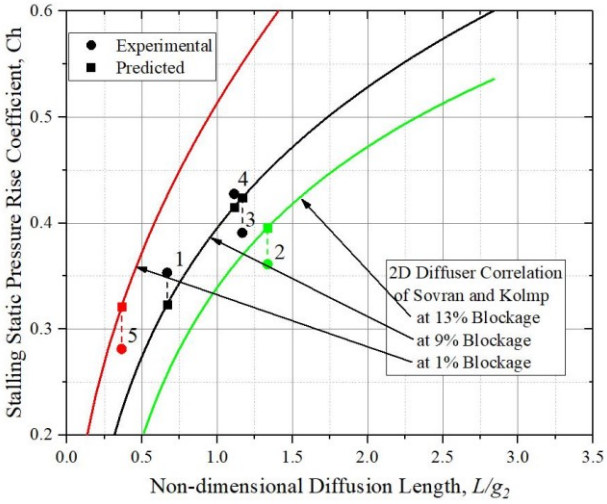

Figure 12. Predicted results of modified stall prediction model

Fig. 11 gives the comparison of the maximum static-pressure-rise coefficient predicted by Koch's model with the test data. It is clear that Koch's model overestimates the maximum pressure rise capability of these axial compressor stages. By considering the effect of flow angles on diffusing, the modified non-dimensional diffusion length is significantly reduced, resulting in a reduction in the predicted pressure rise coefficient and thus more consistent with experimental data. The proposed blockage indicator *BL* also allows a good identification of which curve in Fig. 12 should be used as the correlation for the stall pressure rise.

In order to validate the reliability of the proposed stall prediction model in the multistage environment, the stalling static-pressure-rise coefficient correlation was compared to data from Shanghai Jiao Tong University 4-stage Low Speed Research Compressor (LSRC)[47, 48]. A photo of the LSRC is shown in Figure 13. This is a 1.5-m-tip-dia compressor having an inlet guide vane and four repeating stages. The third stage is the test stage for obtaining detailed internal flow characteristics, the other three stages are used to simulate the multistage environment. The rotating speed is 900 RPM, so the flow is incompressible. The rotating axis of the LSRC is vertical to ensure the circumferential uniformity of the compressor tip clearances. The facility is driven by an AC-

motor with 400 kW maximum power. The detailed design parameters and experimental measurement of the LSRC are described in reference [47 and 48].

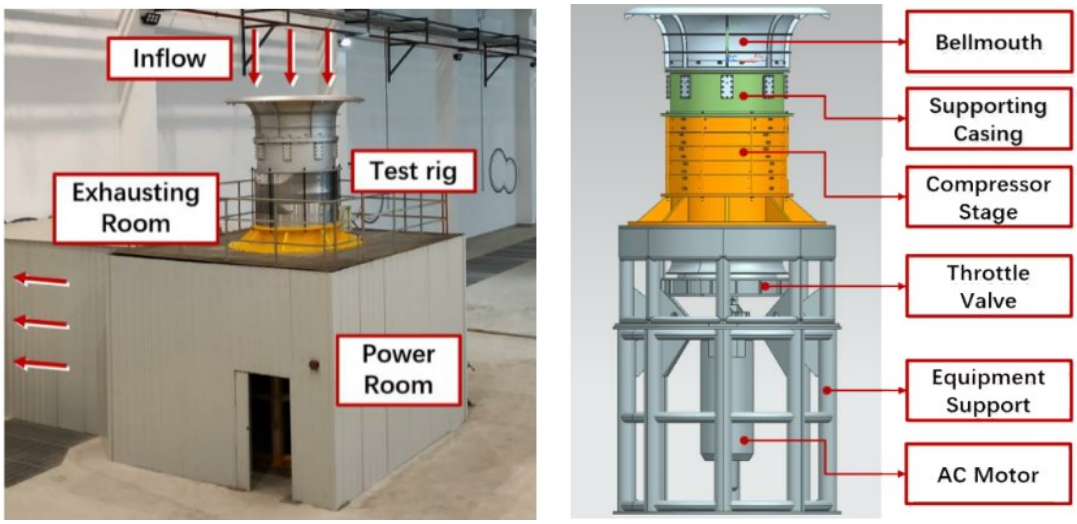

Figure 13. Sketch of Shanghai Jiao Tong University low speed research compressor

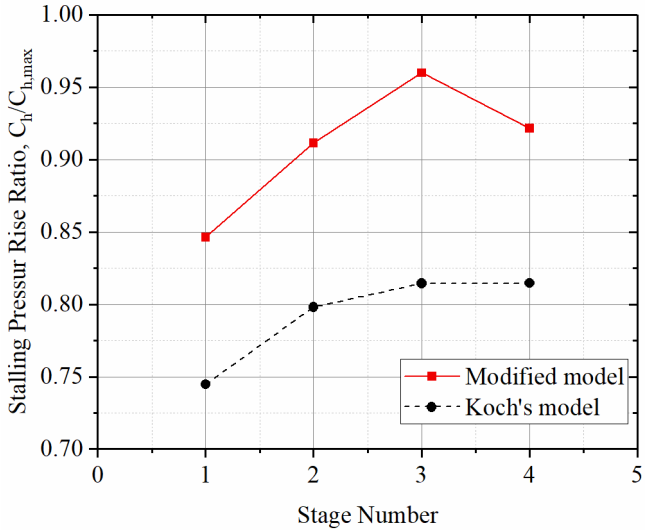

Figure 14. Stagewise distributions of static-pressure-rise ratio for LSRC

In Figure 14, the experimental static-pressure-rise coefficients for each stage of LSRC were ratioed by the stage's predicted values from the modified and Koch's models. The LSRC was operating at near stall (NS) condition at design speed, as shown in Fig.15, thus all stages were not loaded up to the level of the modified correlation. The static-pressure-rise ratio of the third stage is 0.96, which indicates that it is the stall limiting stage in the LSRC. This is because the stator of the third stage is a highly loaded design, while the front and rear stages are matched so as to operate well below the predicted limit of the correlation. It can be seen that the relative error of this model for predicting the stall static pressure rise is only 4%, while the relative error of the original Koch model is 19%, thus compared with the Koch model, the prediction accuracy has been greatly improved.

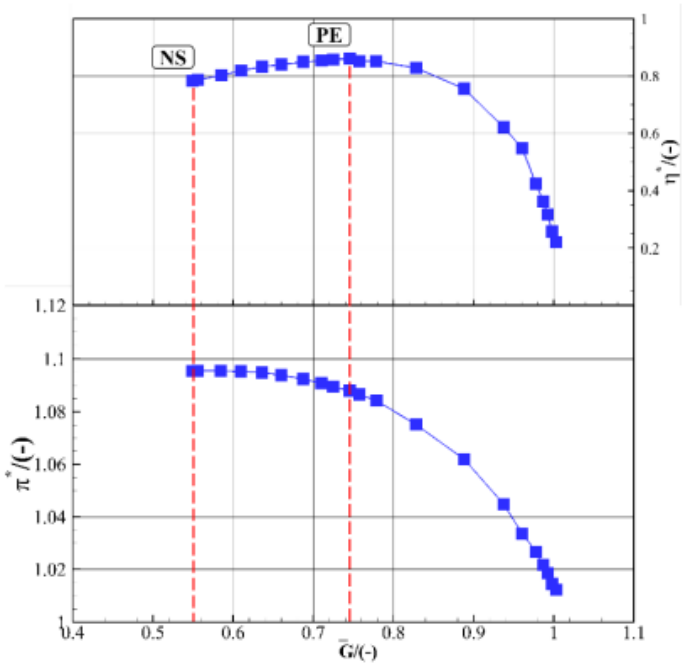

Figure 15. Performance of SJTU-LSRC

6. Conclusions

A correlation for predicting the maximum static-pressure-rise attainable in axial flow compressor stages was developed from about 20 axial compressor stages data utilizing the two-dimensional diffuser analogy concept. The non-dimensional diffusion length was modified to account for the effect of flow angles on the stall pressure rise capability. Here, different from the original Koch's model, the flow angles in Koch' model were only used to consider the increase of effective dynamic factor caused by the high stagger angle. And the mathematical expression for the modified diffusion length was derived in detail in this paper. It was shown that the stalling static-pressure-rise coefficients versus the modified diffusion length were very close to the trend of correlations for two-dimensional diffuser using 1%, 9% and 13% inlet blockage. In addition, Koch put forward that the camber angle has little effect on stalling static-pressure-rise at a fixed stagger angle. In contrast, the results of this paper indicated that the camber angle has a certain influence on the stall capacity of the compressor. And the data scatter could be further removed by adjusting the stalling static-pressure-rise coefficient to the value expected at a reference camber angle. By re-evaluating the effect of Reynolds number on the stalling pressure rise, the proposed blockage indicator could well determine which two-dimensional diffuser performance curve should be used as the stall limit for compressor stages. The comparison of the predicted static-pressure-rise coefficients with the experimental values for a 4-stage low speed research compressor shows that the proposed model can provide a useful estimate of the maximum pressure rise attainable for multistage compressor. For the compressor stages used in this paper, the accuracy of the stall prediction model proposed in this paper is improved from 78% of the original model to 95%.

The stall prediction correlation developed here is obviously a part of a more general model. To complete, more experimental data must be collected and correlated to Generalize the blockage factor, particularly data on low Reynolds number multistage axial compressors. However, due to the limited compressor data that can be obtained, it can only correspond to these three curves at present.

Based on the successful correlation of this paper, the model in its current form is applicable for stall prediction of axial compressor stages during the preliminary design phases.

NOMENCLATURE

BL	blockage indicator
C	blade chord
C_h	static-pressure-rise coefficient
D	diffusion factor
F	correction factor
g	staggered spacing between adjacent blades
k	isentropic coefficient
L	diffusion length in compressor cascade
N	diffusion length in two dimensional diffuser
p	static pressure
R	radius
Re	Reynolds number
S	tangential spacing between adjacent blades
T	static temperature
U	blade speed
V	absolute velocity
W	relative velocity
α	absolute flow angle
β	relative flow angle
κ	blade angle
σ	solidity
ϕ	camber angle
ε	tip clearance
ζ	stagger angle
Δz	axial clearance

Superscripts and subscripts

1	inlet
2	outlet
min	minimum
max	maximum
act	actual

Funding

The author(s) disclosed receipt of the following financial support for the research, authorship, and/or publication of this article: This work was supported by the Natural Science Foundation of China (No. 52076129), National Science and Technology Major Project (2017-II-0004-0017), the United Innovation Center (UIC) of Aerothermal Technologies for Turbomachinery, Innovation Fund from Engineering Research Center of Aerospace Science and Technology, Ministry of Education, and Fund from China Scholarship Council.

Reference

1. Greitzer EM. Review—Axial Compressor Stall Phenomena. ASME. J. Fluids Eng. June 1980; 102(2): 134–151. https://doi.org/10.1115/1.3240634

2. Day IJ. Stall, Surge, and 75 Years of Research. ASME. J. Turbomach. January 2016; 138(1): 011001. https://doi.org/10.1115/1.4031473

3. McDougall NM, Cumpsty NA and Hynes TP. Stall Inception in Axial Compressors. ASME. J. Turbomach. January 1990; 112(1): 116–123. https://doi.org/10.1115/1.2927406

4. Day IJ. Stall Inception in Axial Flow Compressors. ASME. J. Turbomach. January 1993; 115(1): 1–9. https://doi.org/10.1115/1.2929209

5. Guan D, Sun D, Xu R, et al. Experimental investigation on axial compressor stall phenomena using aeroacoustics measurements via empirical mode and proper orthogonal decomposition methods. Aerosp. Sci. Technol. 112(2021): 106655. https://doi.org/10.1016/j.ast.2021.106655

6. Li H, Zheng Q, Chen Z, et al. The role of radial secondary flow in the process of rotating stall for a 1.5-stage axial compressor. Aerosp. Sci. Technol. 115(2021): 106752. https://doi.org/10.1016/j.ast.2021.106752

7. Liu Y, Li J, Du J, et al. Reliability analysis for stall warning methods in an axial flow compressor. Aerosp. Sci. Technol. 115(2021): 106816. https://doi.org/10.1016/j.ast.2021.106816

8. Taddei SR. A novel blade force approach to two-dimensional meanline simulation of transonic compressor rotating stall. Aerosp. Sci. Technol. 111(2021): 106509. https://doi.org/10.1016/j.ast.2021.106509

9. Zhu M, Teng J and Qiang X. Unsteady near-stall flow mechanisms in a transonic compressor rotor at different rotating speeds. Aerosp. Sci. Technol. 119(2021): 107124. https://doi.org/10.1016/j.ast.2021.107124

10. Emmons H. Compressor surge and stall propagation. *Trans of the ASME* 1955; 77: 455-467.

11. Takata H and Nagano S. Nonlinear Analysis of Rotating Stall. ASME. J. Eng. Power. October 1972; 94(4): 279–293. https://doi.org/10.1115/1.3445683

12. Stenning AH. Stall propagation in cascades of airfoils. ASME. Trans. ASME. May 1958; 80(4): 777–789. https://doi.org/10.1115/1.4012510

13. FABRI J and SIESTRUNCK R. Rotating stall in axial flow compressors. J. aeronaut. sci. 24(1970): 805-812.

14. Zika VJ. Correlation and Prediction of Rotating Stall Inception by Divergence Method. ASME. J. Fluids Eng. June 1985; 107(2): 191–196. https://doi.org/10.1115/1.3242459

15. Lieblein S. Loss and stall analysis of compressor cascades. ASME. J. Basic Eng. September 1959; 81(3): 387–397. https://doi.org/10.1115/1.4008481

16. Jiabin L and Lucheng J. An improved prediction model for corner stall in axial compressors

with dihedral effect. Chinese J. Aeronaut . 33(2020): 1433-1443. https://doi.org/10.1016/j.cja.2019.12.031

17. Lei V-M, Spakovszky ZS and Greitzer EM. A Criterion for Axial Compressor Hub-Corner Stall. ASME. J. Turbomach. July 2008; 130(3): 031006. https://doi.org/10.1115/1.2775492

18. Liu B, Fu D and Yu X. Maximum Loading Capacity of Tandem Blades in Axial Compressors. Proceedings of the ASME Turbo Expo 2018: Turbomachinery Technical Conference and Exposition. Volume 2C: Turbomachinery. Oslo, Norway. June 11–15, 2018. V02CT42A044. ASME. https://doi.org/10.1115/GT2018-76770

19. Yu X and Liu B. A Prediction Model for Corner Separation/Stall in Axial Compressors. Proceedings of the ASME Turbo Expo 2010: Power for Land, Sea, and Air. Volume 7: Turbomachinery, Parts A, B, and C. Glasgow, UK. June 14–18, 2010. pp. 211-222. ASME. https://doi.org/10.1115/GT2010-22453

20. De Haller P. Das verhalten von tragflügelgittern in axialverdichtern und im windkanal. Brennstoff-Wärme-Kraft (BWK) 1953; 5: 24.

21. Koch CC. Stalling Pressure Rise Capability of Axial Flow Compressor Stages. ASME. J. Eng. Power. October 1981; 103(4): 645–656. https://doi.org/10.1115/1.3230787

22. Schweitzer JK and Garberoglio JE. Maximum loading capability of axial flow compressors. J Aircr. 1984; 21(8): 593-600. https://doi.org/10.2514/3.45028

23. Smith, Leroy H. , Jr. Axial Compressor Aerodesign Evolution at General Electric. ASME. J. Turbomach. July 2002; 124(3): 321–330. https://doi.org/10.1115/1.1486219

24. Reneau LR, Johnston JP and Kline SJ. Performance and Design of Straight, Two-Dimensional Diffusers. ASME. J. Basic Eng. March 1967; 89(1): 141–150. https://doi.org/10.1115/1.3609544

25. Sovran G. Experimentally determined optimum geometries for rectlinear diffusers with rectangular, conical or annular cross section. Fluid mechanics of internal flow 1967: 270-319.

26. White FM. Fluid mechanics. Tata McGraw-Hill Education, 1979.

27. Kovich G, Tysl ER and Moore RD. Performance of low-pressure-ratio fan stage at two off-design blade setting angles. NASA TM X-3447, 1977.

28. Lewis, Osborn WM and Moore RD. Overall and blade element performance of a 1.20-pressure-ratio fan stage with rotor blades reset -5 deg. NASA TM X-3338, 1976 .

29. Lewis and Tysl ER. Overall and blade-element performance of a 1.20-pressure-ratio fan stage at design blade setting angle. NASA TM X-3101, 1974.

30. Lewis GW and Kovich G. Overall and blade element performance of a 1.20 pressure ratio fan stage with rotor blades reset -7°. NASA TM X-3342,1976.

31. Kovich G and Reid L. Overall and blade-element performance of a transonic compressor stage with multiple-circular-arc blades at tip speed of 419 meters per second. NASA TM X-2731, 1973.

32. Lewis GW, Reid L and Tysl ER. Design and performance of a high- pressure -ratio, highly loaded axial-flow transonic compressor stage. NASA TM X-3100, 1974.

33. Moore RD and Reid L. Performance of a single-stage axial-flow transonic compressor stage with a blade tip solidity of 1.7. NASA TM X-2658, 1972.

34. Schmidt JF and Ruggeri RS. Performance with and without inlet radial distortion of a transonic fan stage designed for reduced loading in the tip region. NASA TP 1294, 1978.

35. Cunnan WS, Stevans W and Urasek DC. Design and performance of a 427-meter-per-second-tip-speed two-stage fan having a 2.40 pressure ratio. NASA TP 1314, 1978.

36. Moore RD and Reid L. Performance of single-stage axial-flow transonic compressor with rotor

and stator aspect ratios of 1.63 and 1.77, respectively, and with design pressure ratio of 2.05. NASA TP 1659, 1980.

37. Moore RD and Reid L. Performance of single-stage axial-flow transonic compressor with rotor and stator aspect ratios of 1.63 and 1.78, respectively, and with design pressure ratio of 1.82. NASA TP 1974, 1982.

38. Osborn WM, Moore RD and Steinke dRJ. Aerodynamic performance of a 1.35-pressure-ratio axial-flow fan stage. NASA TP 1299, 1978.

39. Reid L and Moore RD. Performance of Single-Stage Axial-Flow Transonic Compressor With Rotor and Stator Aspect Ratios of 1.19 and 1.26, Respectively, and With Design Pressure Ratio of 1.82. NASA TP 1338, 1978.

40. Moore RD and Reid L. Performance of Single-Stage Axial-Flow Transonic Compressor With Rotor and Stator Aspect Ratios of 1.63 and 1.77, Respectively, and With Design Pressure Ratio of 2.05. NASA TP 2001, 1982.

41. Urasek DC, Gorrell WT and Cunnan WS. Performance of two-stage fan having low-aspect-ratio first-stage rotor blading. NASA TP 1493, 1979.

42. Cheatham JG, Smith JD and Wright DL. Single-stage experimental evaluation of low aspect ratio, highly loaded blading for compressors. Part 9: Stage F and stage G. Volume 2: Data supplement. NASA CR-134994, 1976.

43. Flynn JT, Keenan MJ and Sulam DH. Single-stage evaluation of highly-loaded high- Mach-number compressor stages. 2 - Data and performance, multiple-circular-arc rotor. NASA CR-72694, 1970.

44. Moore RD and Steinke RJ. Aerodynamic performance of a 1.25-pressure-ratio axial-flow fan stage. NASA TM X-3083, 1974.

45. Morris AL, Halle JE and Kennedy E. High-loading, 1800 ft/sec tip speed transonic compressor fan stage. 1: Aerodynamic and mechanical design. NASA CR-120907, 1972.

46. Osborn WM and Steinke RJ. Performance of a 1.15-pressure-ratio axial-flow fan stage with a blade tip solidity of 0.5. NASA TM X-3052, 1974.

47. Ju Z, Teng J, Zhu M, et al. Flow characteristics on a 4-stage low-speed research compressor with a cantilevered stator. Aerosp. Sci. Technol. 105(2020): 106033. https://doi.org/10.1016/j.ast.2020.106033

48. Zhu M, Qiang X, Ju Z, et al. Experimental and Numerical Researches in a Four-Stage Low Speed Research Compressor Facility. Proceedings of the ASME Turbo Expo 2020: Turbomachinery Technical Conference and Exposition. Volume 2A: Turbomachinery. Virtual, Online. September 21–25, 2020. V02AT32A075. ASME. https://doi.org/10.1115/GT2020-16239